Research Article Vol. 5, No. 5 / May 2018 / Optica 551

Particle trapping and conveying using an optical Archimedes' screw

Barak Hadad,[1,2,†] Sahar Froim,[1,2,†] Harel Nagar,[2,3] Tamir Admon,[2,3] Yaniv Eliezer,[1,2] Yael Roichman,[2,3] and Alon Bahabad[1,2,*]

[1]Department of Physical Electronics, School of Electrical Engineering, Fleischman Faculty of Engineering, Tel-Aviv University, Tel-Aviv 69978, Israel
[2]Tel-Aviv University Center for Light-Matter-Interaction, Tel Aviv 6997801, Israel
[3]School of Chemistry, Raymond and Beverly Sackler Faculty of Exact Sciences, Tel Aviv University, Tel Aviv 69978, Israel
*Corresponding author: alonb@eng.tau.ac.il

Received 18 December 2017; revised 11 March 2018; accepted 27 March 2018 (Doc. ID 314918); published 2 May 2018

Trapping and manipulation of particles using laser beams has become an important tool in diverse fields of research. In recent years, particular interest has been devoted to the problem of conveying optically trapped particles over extended distances either downstream or upstream of the direction of photon momentum flow. Here, we propose and experimentally demonstrate an optical analog of the famous Archimedes' screw where the rotation of a helical-intensity beam is transferred to the axial motion of optically trapped micrometer-scale, airborne, carbon-based particles. With this optical screw, particles were easily conveyed with controlled velocity and direction, upstream or downstream of the optical flow, over a distance of half a centimeter. Our results offer a very simple optical conveyor that could be adapted to a wide range of optical trapping scenarios.

OCIS codes: (350.4855) Optical tweezers or optical manipulation; (140.7010) Laser trapping; (140.3300) Laser beam shaping.

https://doi.org/10.1364/OPTICA.5.000551

1. INTRODUCTION

Optical trapping and translation of particles using focused laser beams has become an important and useful tool in various disciplines such as biology, atomic physics, optics, thermodynamics, and atmospheric sciences [1–6]. For weakly absorbing, sub-wavelength particles, optical trapping and manipulation is based on the interplay of two forces that act on the trapped particles, both of which are caused by radiation pressure [1]. The first force depends on the gradient of the light's intensity, which attracts the particle toward the focal point of the beam. The second force is the scattering force, which usually pushes the particle downstream along the beam's direction of propagation (in special arrangements, the scattering force can be set to pull particles against the momentum flow [7]). These two forces need to counteract each other in order to obtain a stable optical trap. With absorbing particles, the photophoretic force becomes dominant. The photophoretic force is proportional to particle size and the light's intensity. This force is thermal in nature, namely, when light hits one side of a particle, that side becomes warmer, increasing the pressure of the nearby air molecules. The resulting pressure drop between the warm and cold sides of the particle pushes them downstream, and away from the light. This force tends to repel an absorbing particle from high-intensity regions of an optical beam. It has been shown that the ratio of photophoretic forces and radiation pressure forces for absorbing sub-wavelength particles is close to 10^4 [8]. Therefore, for such particles, radiation pressure forces can be neglected, whereas photophoretic force governs particle transportation up to a meter length scale [9]. Special interest is devoted to developing optical tractor beams, which allow the transfer of particles against the direction of the beam's propagation, i.e., the direction of the beam's momentum. This poses an interesting challenge since it requires moving a particle against the direction of both photophoretic forces and radiation pressure forces when a simple Gaussian beam is used. In addition to moving particles upstream, such tractor beams, also known as optical conveyors, are generally required to transport particles in both directions, upstream and downstream, in a controlled manner. For weakly absorbing particles, in a solution, optical conveyors were realized using a superposition of two Bessel beams, while changing the relative phase between them [10]. This change in phase shifts the standing-wave pattern of the structured beam, carrying along particles trapped at the standing-wave intensity crests. For airborne absorbing particles that are expelled from high-intensity regions, the common practice is to use hollowed beams with dark volumes to trap the particles and then move the dark volume [11,12]. Alternatively, particles were manipulated by changing the polarization of the beam [13]. For asymmetric airborne particles, it was shown experimentally that the axial location of a trapped particle can be controlled by changing the intensity of a single Gaussian beam [14]. Many of the beams

used in optical trapping use spatial modes with orbital angular momenta (OAMs) [15–18]. These modes enable both the generation of hollowed beams useful in trapping absorbing airborne particles [9,13,19,20] and the transportation of particles along helical trajectories [21,22].

Here we present, experimentally, the use of a helical beam, made from the superposition of modes with different OAMs and different axial wave vector components, to trap and transport absorbing airborne particles up- and downstream by rotating the beam one way or the other. This technique is an optical realization of the famous Archimedes' screw, used to draw water from underground wells. Not too close to the focus of the beam, the particle motion is matched to the movement of the optical screw, enabling robust and scalable two-way conveying. We would like to note that in recent years, an optical Archimedes screw was suggested for manipulating the movement of trapped cold atoms [23,24].

2. RESULTS

A. Experimental Setup

The experimental setup (see Fig. 1) is driven with a 532 nm CW laser (Laser Quantum Ventus 532 Solo) and uses a reflective phase-only spatial light modulator (SLM) (Holoeye Pluto SLM). The laser beam is expanded and collimated, reflected off the SLM, demagnified using a collimating telescope, and finally focused using a 5 cm focal lens into a cuvette containing aerosol carbon nanoparticles (ALDRICH Carbon nanopowder; <100 nm particles). Observing the particles under a microscope, we see an average diameter of 1.4 μm, suggesting that we are actually trapping aggregates. The power of the laser after the focusing lens that was used is 53 mW (stable trapping was observed for powers down to ∼30 mW). The trapped particles inside the cuvette were imaged using an LG G3 smartphone camera (13 MP, $f/2.4$, 29 mm, phase detection/laser autofocus) and also using a scientific CMOS camera (Ophir Spiricon SP620U Beam Profiling Camera) on a translation stage aligned parallel to the optical axis of the beam. The same camera was also used together with a magnifying imaging lens (focal length 5 cm), on a translation stage, in front of the beam with various filters to capture the beam profile together with a trapped particle while a 633 nm laser (with intensity on the trapped particle much smaller than that of the trapping laser) illuminates the trapped particle from the side. Different phase patterns with relative rotation of $2\pi/M$ (with $M = 50$) were used to rotate the beam. The phase patterns were projected sequentially by the SLM, at a controlled rate, setting the beam's rotation velocity. Particle motion was extracted from raw film footage by first increasing the image contrast and then using the Hough transform [25] for feature extraction.

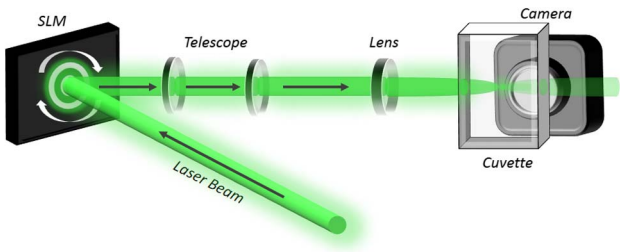

Fig. 1. Experimental setup. A collimated laser light reflects off a SLM, is scaled down using a telescope, and finally focused into a cuvette filled with airborne absorbing particles. A camera records the motion of the trapped particles.

B. Construction of the Optical Screw

The optical Archimedes' screw is a standing wave with a helical intensity profile. Several works show that a helical intensity profile can be generated by superposing modes with different OAMs and different linear momenta [26–34]. Similarly, in our case, the optical screw is constructed from a superposition of two beams carrying different linear and angular momenta. Basically, a superposition of modes characterized by different momenta results in a standing wave in the conjugate coordinate. This is true whether the conjugate pair is linear momentum and linear coordinate or angular momentum and azimuthal coordinate. Thus, the superposition of two spatial modes that differ in both their linear and angular momenta would result in a standing-wave pattern in both the longitudinal and azimuthal directions with the overall effect of realizing a helical intensity profile. The modes we use are based on ideal Bessel beams described with [35,36] $E(r,\phi,z) = A_0 e^{ik_z z} J_n(k_r r) e^{\pm in\phi}$, where A_0 is an arbitrary field amplitude; k_z and k_r are the wave number components in the longitudinal and transverse directions, respectively; $J_n(x)$ is the Bessel function of the nth order; and n is a dimensionless integer (known as topological charge) representing the OAM quantized in units of $\hbar$ per photon [16–18]. When $n > 0$, such a mode is known as a vortex Bessel beam.

The spectral representation of such an ideal beam is an infinitely thin ring of uniform intensity and an azimuthally linear phase profile with an nth order rotational symmetry [37]. The radius of the ring sets the value of the longitudinal linear momentum. In our case, we create a superposition of two non-ideal vortex Bessel beams in Fourier space by using two finite-thickness rings, with different radii and opposing phase profiles, characterized by $n = \pm 1$. We then multiply the phase pattern with a blazed phase grating so that only light that is reflected off the ring area is directed into the first diffraction order of the grating. To realize this pattern physically, we use a phase-only SLM in a $2f$ configuration. The phase pattern realized on the SLM is shown in Fig. 2(a). The measured beam cross section after magnification and a $2f$ Fourier transform at the focal plane of the lens agrees well with its expectation [compare Figs. 2(b) and 2(c)]. Its evolution along the axial direction is shown in Fig. 2(d). We note that the experimentally measured beam cross section was taken using a longer focal lens to improve resolution. A calculation using Fresnel field propagation shows iso-intensity surfaces of the beam in a volume around the focal plane [see Fig. 2(e)]. Here, the pitch of the screw is half its axial period, whereas generally, for a similar beam constructed from two modes with charges of $\pm n$, the ratio between period and pitch is $2n$:1. The condition with which the pitch Λ can be calculated is $I(r,\phi,z+\Lambda) = I(r,\phi,z)$, where I is the intensity of the beam. The condition for calculating the period Δz is $I(r,\phi,z+\Delta z) = I(r,\phi+2\pi,z)$. The pitch is fixed by the radii of the rings on the SLM and is given by $\Lambda = \lambda \cdot [\cos(\theta_1) - \cos(\theta_2)]^{-1}$, where $\theta_i = \tan^{-1}(\frac{R_i}{f})$, with R_i the radius of each ring on the mask and f the focal length of the lens. Switching the sign of the topological charge associated with each ring would switch the helicity of the whole beam.

Each of the vortex Bessel beams is approximately non-diffracting along a length of $L_{\mathrm{ND}} = 2\lambda f^2/(WR)$ [38], where W is the width of the ring and R is its radius. The optical screw

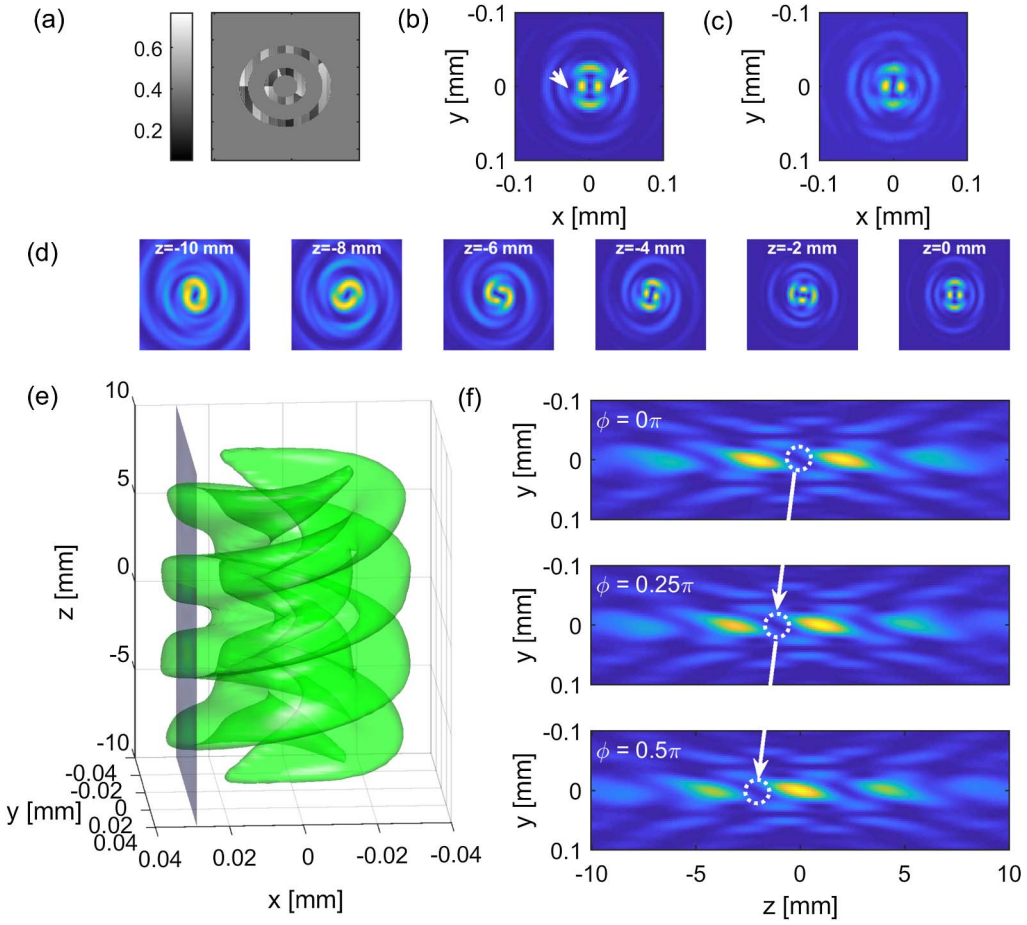

Fig. 2. Optical Archimedes' screw. (a) The Fourier domain mask that was applied to the phase-only SLM. (b) Calculation of beam profile in the focal plane at the middle of the cuvette. The arrows indicate dark volumes in which particles were observed to be trapped. (c) Beam profile captured on a camera, using a lens of a longer focal length than used for trapping, and scale-adjusted for the lens used for trapping. (d) Calculation of beam profile at several locations along the propagation length. (e) Simulation of several iso-intensity surfaces of the beam around the focal plane. (f) Simulations, for several rotation angles ϕ of the optical screw, of a plane cut [as shown in (e)] of the beam parallel to the optical axis and displaced transversely to the point indicated by one of the arrows on panel (b) above. The dashed white circles denote a possible trap location for the particle. The white arrows are a guide to the eye.

retains its form along this length, but starts to broaden further upstream or downstream due to diffraction. The central part of the beam is composed of $2n$ intertwining strands. A rotation of the optical screw around the propagation axis is easily accomplished by rotating either one or both of the rings on the SLM. In the first case, the interference pattern is rotating, whereas in the second, it is the whole beam. The overall effect is similar, with the difference (for the case $n = 1$) that a $\Delta\theta$ rotation of one of the rings is the same as rotating the whole beam by $\Delta\theta/2$. When a particle is trapped at one of the off-axis dark volumes in the beam, it is carried upstream or downstream depending on the direction of beam rotation and beam helicity (which is constant in our experiment).

C. Screw-Velocity-Matched Particle Motion

A particle trapped in the optical screw maintains its position as long as the screw is stationary. The trapping stiffness is estimated to be around 50 pN/m (see Supplement 1). When the screw is rotating, the trapped particle is translated in a controlled manner, as long as it remains far enough from the focal plane of the beam (1 mm away in our case), and is driven at velocities lower than ~0.3 mm/s. The axial movement of the particle in these cases is close to the axial phase velocity of the optical screw, defined as the screw period divided by the screw's rotation time period. The particle is repelled from the high-intensity regions of the rotating beam, very similarly to water or air molecules being repelled from the blades of a rotating fan. The small diffraction of the screw is responsible for the difference between the actual axial velocity of the particle and the calculated phase velocity (which is exact only for an infinitely non-diffracting beam). Still we describe this type of movement as screw-velocity-matched movement.

As a demonstration, we accomplish periodic oscillatory motion of trapped particles by repeatedly rotating the screw one way, and then the other. This oscillatory motion is repeated with two different rotation speeds and with different number of rotations of the screw to each side. The axial (z direction) movement of the trapped particles for these cases are shown in Fig. 3. The two phase velocities we used are 0.08 mm/s [Figs. 3(a) and 3(c)] and 0.04 mm/s [Figs. 3(b) and 3(d)]. The number of screw rotations we used to each side was half a turn [$N = 0.5$; Figs. 3(a) and 3(b)] and three quarters of a turn [$N = 0.75$; Figs. 3(c) and 3(d)]. In total, we then have four different movements of the screw and

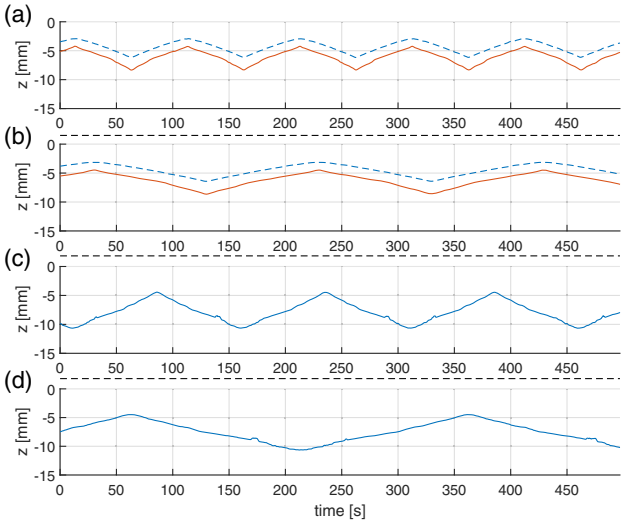

Fig. 3. Screw-velocity-matched particle axial motion. In all cases, the optical screw is periodically switching its rotation direction after N rotations and its axial phase velocity is v_p. (a) $N = 0.5$, $v_p = 0.08$ mm/s. (b) $N = 0.5$, $v_p = 0.04$ mm/s. (c) $N = 0.75$, $v_p = 0.08$ mm/s. (d) $N = 0.75$, $v_p = 0.04$ mm/s. Two particles were trapped together in cases (a) and (b). The coordinate $z = 0$ marks the focal plane of the beam.

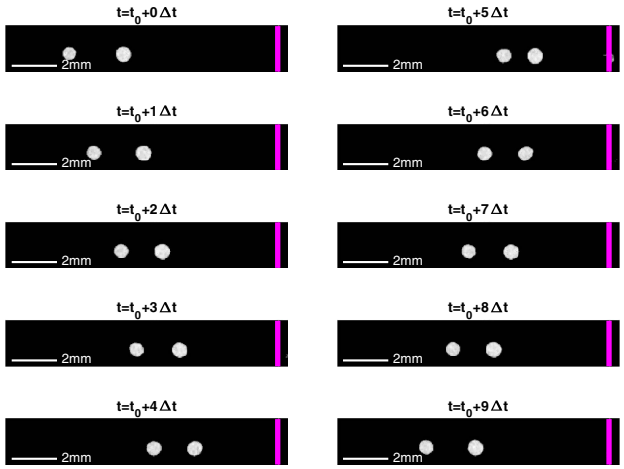

Fig. 4. Camera snapshots during the oscillatory movement of two particles trapped together in a rotating optical screw. During the interval that the snapshots were taken, the optical screw is first rotating to move the particles upstream (left) and then downstream (right). The phase velocity of the optical screw is $v_p = 0.08$ mm/s. The two particles are trapped at an average distance of 2 mm from each other. The focal plane is marked with a vertical (purple) line on the right-hand side of each image. t_0 was set to a moment just after a change of direction of particle movement. $\Delta t = 10$ s.

the trapped particle is locked and velocity-matched to this movement. The pitch of the screw in all cases was 4.1 mm (The parameters of the optical screw were chosen to create about two full turns of the screw within the confines of the cuvette whose length along the optical axis is 2 cm). Incidentally, for the cases shown in Figs. 3(a) and 3(b), two particles were trapped at the same time at two different axial locations of the screw (separated by 2 mm). It can be seen that they move in tandem performing similar motion. Using a magnifying imaging system, it was verified (with an error of ± 0.44 μm) that the particles do not move along the transverse directions, while their location within the beam profile is set off-axis as indicated using an arrow in Fig. 2(b). As the particles are transversely displaced off-axis, they experience an intensity landscape that moves axially as the screw is being rotated. This can be appreciated by examining, for different rotations of the optical screw, a plane cut of the beam whose location is parallel to the optical axis and displaced off-axis to the position of the trapped particles [see Fig. 2(f)].

We would like to note that, since the beam retains some slow divergence (it is not perfectly non-diffracting), the axial velocity of the conveyed particles is slightly dependent on the axial position of the particles. This can be seen for the two particles moving in tandem in Figs. 3(a) and 3(b), where due to their different axial positions, their axial velocities are also slightly different and so the distance between them changes along their trajectories. This can be seen more clearly in Fig. 4 showing camera snapshots for the pair of particles during an oscillation of their movement (see also Visualization 1 for a video of this motion).

D. Periodic Particle Motion with Non-Matched Velocities

When particles are brought close to the focal plane of the beam (in our case, about 1 mm from the focus) by rotation of the optical screw, their velocities do not continuously match the phase velocity of the optical screw, and their motions exhibit complex periodic behavior. In such cases, the nature of the motion is sensitive to both the rotation dynamics of the optical screw and the location of the particles with respect to the focal plane. However, all motions we have tracked exhibit periodic oscillatory behavior, regardless if the screw rotation is constant or switching directions. In Figs. 5(a) and 5(b), the screw was rotating continuously along the beam direction (striving to deliver particles downstream) at

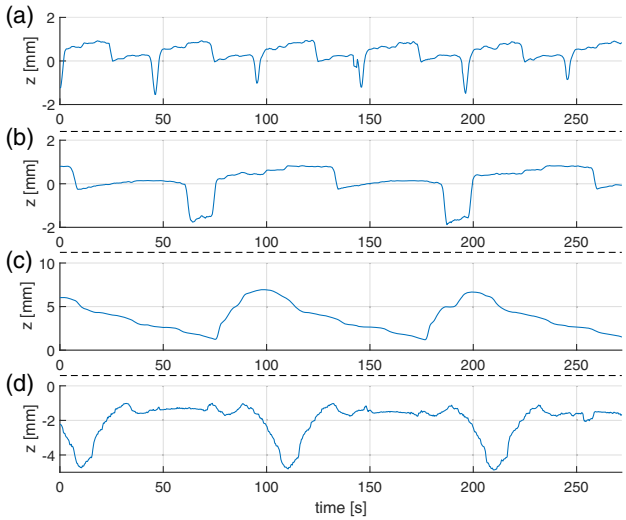

Fig. 5. Non velocity-matched periodic particle axial motion. (a) The optical screw is constantly rotating to deliver particles downstream at a phase velocity of $v_p = 0.08$ mm/s and a pitch of 4.1 mm. (b) Downstream, $v_p = 0.03$ mm/s, pitch 4.1 mm. (c) Upstream, $v_p = 0.08$ mm/s, pitch 4.1 mm. (d) The direction of optical screw rotation is switched every half a turn (every pitch cycle); $v_p = 0.23$ mm/s, pitch 11.3 mm. The coordinate $z = 0$ marks the focal plane of the beam.

velocities of 0.08 and 0.03 mm/s, respectively, with a pitch of 4.1 mm. In both cases, the particle crossed the focal plane of the beam, lingering for a relatively large portion of its period very close to the focus. Eventually it was pushed back and then carried again toward the focus, where it lingered again and so on. In Fig. 5(c), the screw was rotating continuously against the beam direction with a velocity of 0.08 mm/s and a pitch of 4.1 mm, aiming to move the particle upstream. In this case, the particle was unable to cross the focal plane. While it was being carried toward the focus, it moved together with the screw phase velocity, but once it arrived close to the focal plane, it was pushed, relatively rapidly, downstream, up to a point where the optical field of the screw was able to trap and carry it again upstream.

Finally, in Fig. 5(d), the motion of the optical screw is oscillatory—rotating half a turn to each side at a phase velocity of 0.23 mm/s with a pitch of 11.3 mm. In this case, the particle is carried toward or away from the focal plane at a velocity of 0.22 mm/s locked to the phase velocity of the optical screw. However, when it comes close to the focal plane, it lingers for a long time at a specific axial position. The particle is able to escape only when the screw force is directed to pull it out, upstream. In all cases described here, the motion of the trapped particle is no longer velocity-matched at all times to the motion of the optical screw. However, the motion is still locked to the rotation of the optical screw in the sense that the periodicities of the various motions described here are equal to that of the optical screw. Namely, the periods of motion of the particles are equal to the rotation period of the optical screw in the cases where the screw is rotating continuously in the same direction, and twice this value when the screw is changing its rotation direction after each full revolution.

We note that the periodic motions observed here are reminiscent of a somewhat similar phenomenon observed lately due to the interplay of photophoretic and direct optical forces [39]. However, here the motion is on a much longer scale and is driven by changing the intensity profile (by rotation) of the light beam.

3. CONCLUSIONS AND DISCUSSION

To conclude, we have experimentally demonstrated the transfer of rotational movement of a helical beam to the axial movement of a trapped particle within the beam, by realizing an optical analog to the famous Archimedes' screw. We observe two regimes of motion depending on the proximity of a trapped particle to the focal plane of the beam. If a trapped particle is located far enough from the focal plane, the motion of the particle is velocity-matched to the movement of the optical screw, whether the axial velocity of the screw is directed upstream or downstream. If the particle is close enough to the focal plane, it exhibits periodic motion locked to the period of the screw rotation; however, its motion is no longer velocity-matched to the motion of the optical screw at all times. The axial amplitude of the motion demonstrated in our setup was about 0.5 cm. However, the simplicity of the method and its basic operation principle suggest that it could be extended to either longer scales or smaller dimensions with better resolution. Furthermore, in contrast to other methods of conveying airborne particles [9,13], where the velocity of particles is dictated by the intensity of the light and the dimensions of the particles, here the velocity is dependent only on the rotation speed of the optical screw. An interesting question is whether this method could be applied to weakly absorbing particles in suspension. In cases where the particles are attracted to the light, rather than repelled from it, we expect that the particles would stick to the helical beam in a given transverse plane, and so, if possible at all, a more elaborate scheme would probably be needed to transfer the particles axially while the helical beam is rotated. Finally, we expect this method to be useful for applications with multiple particles, for example, for the construction of an optical turbine.

Funding. Israel Science Foundation (ISF) (988/17).

Acknowledgment. H. N., T. A., and Y. R. wish to acknowledge support from the ISF.

See Supplement 1 for supporting content.

†These authors contributed equally to this work.

REFERENCES

1. R. W. Bowman and M. J. Padgett, "Optical trapping and binding," Rep. Prog. Phys. **76**, 026401 (2013).
2. M. Daly, M. Sergides, and S. Nic Chormaic, "Optical trapping and manipulation of micrometer and submicrometer particles," Laser Photon. Rev. **9**, 309–329 (2015).
3. M. Dienerowitz, M. Mazilu, and K. Dholakia, "Optical manipulation of nanoparticles: a review," J. Nanophoton. **2**, 021875 (2008).
4. D. G. Grier, "A revolution in optical manipulation," Nature **424**, 810–816 (2003).
5. J. R. Moffitt, Y. R. Chemla, S. B. Smith, and C. Bustamante, "Recent advances in optical tweezers," Annu. Rev. Biochem. **77**, 205–228 (2008).
6. M. Woerdemann, C. Alpmann, M. Esseling, and C. Denz, "Advanced optical trapping by complex beam shaping," Laser Photon. Rev. **7**, 839–854 (2013).
7. O. Brzobohatý, V. Karásek, M. Šiler, L. Chvátal, T. Čižmár, and P. Zemánek, "Experimental demonstration of optical transport, sorting and self-arrangement using a 'tractor beam'," Nat. Photonics **7**, 123–127 (2013).
8. A. S. Desyatnikov, V. G. Shvedov, A. V. Rode, W. Krolikowski, and Y. S. Kivshar, "Photophoretic manipulation of absorbing aerosol particles with vortex beams: theory versus experiment," Opt. Express **17**, 8201–8211 (2009).
9. V. G. Shvedov, A. V. Rode, Y. V. Izdebskaya, A. S. Desyatnikov, W. Krolikowski, and Y. S. Kivshar, "Giant optical manipulation," Phys. Rev. Lett. **105**, 118103 (2010).
10. D. B. Ruffner and D. G. Grier, "Optical conveyors: a class of active tractor beams," Phys. Rev. Lett. **109**, 163903 (2012).
11. P. Zhang, Z. Zhang, J. Prakash, S. Huang, D. Hernandez, M. Salazar, D. N. Christodoulides, and Z. Chen, "Trapping and transporting aerosols with a single optical bottle beam generated by moiré techniques," Opt. Lett. **36**, 1491–1493 (2011).
12. V. G. Shvedov, C. Hnatovsky, A. V. Rode, and W. Krolikowski, "Robust trapping and manipulation of airborne particles with a bottle beam," Opt. Express **19**, 17350–17356 (2011).
13. V. Shvedov, A. R. Davoyan, C. Hnatovsky, N. Engheta, and W. Krolikowski, "A long-range polarization-controlled optical tractor beam," Nat. Photonics **8**, 846–850 (2014).
14. J. Lin and Y.-Q. Li, "Optical trapping and rotation of airborne absorbing particles with a single focused laser beam," Appl. Phys. Lett. **104**, 101909 (2014).
15. L. Allen, M. W. Beijersbergen, R. Spreeuw, and J. Woerdman, "Orbital angular momentum of light and the transformation of Laguerre–Gaussian laser modes," Phys. Rev. A **45**, 8185–8189 (1992).
16. M. Padgett and L. Allen, "Light with a twist in its tail," Contemp. Phys. **41**, 275–285 (2000).
17. M. Padgett, J. Courtial, and L. Allen, "Light's orbital angular momentum," Phys. Today **57**(5), 35–40 (2004).
18. A. M. Yao and M. J. Padgett, "Orbital angular momentum: origins, behavior and applications," Adv. Opt. Photon. **3**, 161–204 (2011).

19. V. Shvedov, A. S. Desyatnikov, A. V. Rode, Y. Izdebskaya, W. Krolikowski, and Y. S. Kivshar, "Optical vortex beams for trapping and transport of particles in air," Appl. Phys. A **100**, 327–331 (2010).
20. V. G. Shvedov, A. S. Desyatnikov, A. V. Rode, W. Krolikowski, and Y. S. Kivshar, "Optical guiding of absorbing nanoclusters in air," Opt. Express **17**, 5743–5757 (2009).
21. S.-H. Lee, Y. Roichman, and D. G. Grier, "Optical solenoid beams," Opt. Express **18**, 6988–6993 (2010).
22. J. Zhao, I. D. Chremmos, D. Song, D. N. Christodoulides, N. K. Efremidis, and Z. Chen, "Curved singular beams for three-dimensional particle manipulation," Sci. Rep. **5**, 12086 (2015).
23. A. Y. Okulov, "Cold matter trapping via slowly rotating helical potential," Phys. Lett. A **376**, 650–655 (2012).
24. A. Al Rsheed, A. Lyras, O. M. Aldossary, and V. E. Lembessis, "Rotating optical tubes for vertical transport of atoms," Phys. Rev. A **94**, 063423 (2016).
25. J. Illingworth and J. Kittler, "A survey of the Hough transform," Comput. Vis. Graph. Image Process. **44**, 87–116 (1988).
26. C. Schulze, F. S. Roux, A. Dudley, R. Rop, M. Duparré, and A. Forbes, "Accelerated rotation with orbital angular momentum modes," Phys. Rev. A **91**, 043821 (2015).
27. C. Vetter, T. Eichelkraut, M. Ornigotti, and A. Szameit, "Generalized radially self-accelerating helicon beams," Phys. Rev. Lett. **113**, 183901 (2014).
28. V. Kotlyar, S. Khonina, R. Skidanov, and V. Soifer, "Rotation of laser beams with zero of the orbital angular momentum," Opt. Commun. **274**, 8–14 (2007).
29. R. Rop, A. Dudley, C. López-Mariscal, and A. Forbes, "Measuring the rotation rates of superpositions of higher-order Bessel beams," J. Mod. Opt. **59**, 259–267 (2012).
30. Y. Y. Schechner, R. Piestun, and J. Shamir, "Wave propagation with rotating intensity distributions," Phys. Rev. E **54**, R50–R53 (1996).
31. S. Tao, X.-C. Yuan, J. Lin, and R. Burge, "Residue orbital angular momentum in interferenced double vortex beams with unequal topological charges," Opt. Express **14**, 535–541 (2006).
32. R. Vasilyeu, A. Dudley, N. Khilo, and A. Forbes, "Generating superpositions of higher-order Bessel beams," Opt. Express **17**, 23389–23395 (2009).
33. S. Zheng, Y. Cai, Y. Li, J. Li, G. Zheng, H. Chen, and S. Xu, "Rotating wave packet caused by the superposition of two Bessel–Gauss beams," J. Opt. **17**, 125602 (2015).
34. A. Dudley and A. Forbes, "From stationary annular rings to rotating Bessel beams," J. Opt. Soc. Am. A **29**, 567–573 (2012).
35. J. Durnin, "Exact solutions for nondiffracting beams. i. The scalar theory," J. Opt. Soc. Am. A **4**, 651–654 (1987).
36. D. McGloin and K. Dholakia, "Bessel beams: diffraction in a new light," Contemp. Phys. **46**, 15–28 (2005).
37. J. Durnin, J. Miceli, Jr., and J. Eberly, "Diffraction-free beams," Phys. Rev. Lett. **58**, 1499–1501 (1987).
38. L. Lobachinsky, L. Hareli, Y. Eliezer, L. Michaeli, and A. Bahabad, "On the fly control of high harmonic generation using a structured pump beam," Phys. Rev. Lett., to be published.
39. J. Lu, H. Yang, L. Zhou, Y. Yang, S. Luo, Q. Li, and M. Qiu, "Light-induced pulling and pushing by the synergic effect of optical force and photophoretic force," Phys. Rev. Lett. **118**, 043601 (2017).